https://doi.org/10.5194/acp-2019-1062
Preprint. Discussion started: 22 January 2020

Atmospheric Chemistry and Physics Discussions

Improved inversion of aerosol components in the atmospheric column from remote sensing data

Ying Zhang[1], Zhengqiang Li[1], Yu Chen[2], Gerrit de Leeuw[3], Chi Zhang[1], Yisong Xie[1], Kaitao Li[1]

[1]State Environmental Protection Key Laboratory of Satellite Remote Sensing, Institute of Remote Sensing and Digital Earth, Chinese Academy of Sciences, Beijing 100101, China
[2]Public Meteorological Service Center, China Meteorological Administration, Beijing 100081, China
[3]Finnish Meteorological Institute, Climate Research, Helsinki FI-00101, Finland

Correspondence to: Zhengqiang Li (lizq@radi.ac.cn)

Abstract. A method to calculate the complex refractive index of a multicomponent liquid system is introduced into the retrieval of atmospheric columnar aerosol components from optical remote sensing data. The aerosol components comprise five species, combining eight sub-components including black carbon (BC), water-soluble (WSOM) and water-insoluble organic matter (WIOM), ammonium nitrate (AN), sodium chloride (SC), dust-like (DU), and aerosol water in the fine and coarse modes (AW_f and AW_c). The uncertainty in the retrieval results is analyzed based on the simulation of typical models, showing that the complex refractive index obtained from instantaneous optical-physical inversion compares very well with that obtained from chemical estimation. The algorithm was used to retrieve the columnar aerosol components over China using the ground-based remote sensing measurements from the Sun-sky radiometer Observation NETwork (SONET) in the period from 2010 to 2016. The results were used to analyze the regional distribution and interannual variation. The analysis shows that the atmospheric columnar DU component is dominant in the northern region of China, whereas the AW is higher in the southern coastal region. The AN significantly decreased from 2011 to 2016, by 26.8 mg m^{-2}, which is inseparable from China's environmental control policies.

1. Introduction

Atmospheric aerosol consists of a suspension of solid and/or liquid particles in the air which scatter and absorb solar radiation. The chemical composition and mixing state of the aerosol particles affect their optical characteristics, which in turn influence the energy budget of the Earth-atmosphere system and thus climate (Boucher et al., 2013).

To measure aerosol composition, many methods are used including online analysis in the field, sample analysis in the laboratory, remote sensing estimation, etc. It is noted, that the detail of information depends on the technique used and the information available. Optical remote sensing techniques do not provide sufficient information for a detailed analysis of chemical composition and therefore refrain to the retrieval of components describing specific properties. Because of fast observation and low cost, the application of remote sensing techniques to estimating aerosol components has developed rapidly since 2000. Satheesh et al. (1999; 2002a, b; 2005) established an algorithm for the inversion of aerosol components from

https://doi.org/10.5194/acp-2019-1062
Preprint. Discussion started: 22 January 2020

remote sensing data based on the hypothesis of external mixing and assuming fixed size distributions for each component. But an external mixture usually cannot accurately describe the natural state of aerosols. Even if the particles are individually pure when first produced, numerous processes in the atmosphere will convert an external mixture to an internal mixture (Lesins et al., 2002). Therefore, internal mixing hypotheses are widely used and multiple approaches have been developed (e.g., Zhang et al., 2018; Schuster et al., 2016, 2009, 2005; van Beelen et al. 2014; Li et al., 2013; Wang et al., 2013; Arola et al., 2011). Schuster et al. (2005) discriminated between black carbon (BC) and non-absorbing components based on the spectral differences using remote sensing measurements. The dust component (DU) was estimated in the study of Schuster et al. (2009) using its typical coarse mode particles and weak absorption of solar light. Brown carbon was further estimated by Arola et al. (2011) due to the large change of its absorbing characteristic with wavelength for wavelengths smaller than 550 nm, but the dust component was ignored in this study. Aerosol bimodal characteristics were used by Schuster et al. (2016) to estimate the aerosol absorbing components including BC, brown carbon and hematite in the fine and coarse modes. This method was also embedded in the GRASP (Generalized Retrieval of Aerosol and Surface Properties) system by Li et al. (2019) for application to POLDER/PARASOL observations. The above algorithms are aimed at retrieving absorbing aerosol components, such as BC, brown carbon and iron oxides, but have only simple treatment for scattering components, especially the host of multicomponent liquids.

van Beelen et al. (2014) introduce water-soluble organic matter (WSOM) in the inversion process based on the hygroscopicity of the OM mixture, but in this study water-insoluble organic matter (WIOM) was not accounted for. Some studies separated the OM based only on the spectral changes (Xie et al., 2017; Choi and Ghim, 2016) leading to large uncertainty in the results. Zhang et al. (2018) simultaneous retrieved the WSOM and WIOM components but ignored the error in the refractive index introduced by the aerosol volume averaging method applied to the multicomponent liquid system. For other non-absorbing components, the water content and inorganic components in the fine mode are identified by the difference in hygroscopic growth between organic and inorganic matter (Zhang et al., 2018; van Beelen et al.; 2014). In the coarse mode, sea salt is identified by the aerosol sphericity in the study of Xie et al. (2017) but this parameter is difficult to observe.

Although the retrieval of aerosol components by using remote sensing methods has been greatly developed, the application of hygroscopicity to identify the weak and non-absorbing components in a multicomponent liquid system remains difficult. In this study, hygroscopicity is introduced to solve the refractive index in a multicomponent liquid system. The results are used in an algorithm to retrieve aerosol components from data obtained from the ground-based remote sensing network SONET (Li et al, 2018). The data and method are described in sections 2 and 3, respectively. The results for the aerosol components and derived hygroscopic parameter and effective density are presented and analyzed in section 4, and we conclude this study in section 5.

https://doi.org/10.5194/acp-2019-1062
Preprint. Discussion started: 22 January 2020

Atmospheric Chemistry and Physics Discussions

2 Measurements

2.1 Sun-Sky radiometer

The multiwavelength polarized sun-sky radiometer CE318-DP manufactured by Cimel Electronique in France, as a highly accurate measuring instrument for long-term continuous observations in the field, can automatically measure solar and sky radiation. It consists of an optical head, a control box and a biaxial stepping motor system. The optical head has two views: one for direct solar radiation with no focusing lens and the other for sky radiation with focusing lens. The internal optical system consists of a spectral and a polarizing filter to measure in different wavebands and polarization directions. The 9 wavebands vary from the visible to the near-infrared (340, 380, 440, 500, 675, 870, 936, 1020, 1640 nm) with a full width at half maximum of 10 nm. All bands provide both radiation and polarization measurements, except the 936 nm band which only measures radiation to determine columnar water vapor. These radiation and polarization measurements can provide much information to calculate the columnar aerosol optical depth (AOD) and further retrieve the aerosol microphysical parameters.

2.2 SONET

The Sun-sky radiometer Observation NETwork (SONET) is a local observation network in China for ground-based remote sensing measurements of aerosols (Li et al., 2018). At present, there are as many as 16 long-term observation sites in China, which are evenly distributed over north and south China, northwest China and the Tibetan Plateau (Figure 1). The geographical and topographic features of the long-term sites are diverse such as plateau, desert, hilly, plain and island, including three megacities, three islands and one plateau site (Table 1). Among the 16 stations, six sites recorded observations for more than five years, and the longest time series of 7 years has been recorded in Beijing. SONET provides sufficient samples, with long-term time series, wide space coverage and diverse climatic and topographic features, for the analysis of atmospheric aerosol characteristics in China.

Continuous observations of direct and sky light are carried out by the multi-wavelength polarization sun-sky radiometer (CE318-DP) in the observation network. Based on the inversion algorithm of Dubovik et al. (2000), more than 20 parameters describing the optical, physical and chemical global properties are retrieved as column-integrated properties (Li et al., 2018), including particle volume size distribution (PVSD), complex refractive index (CRI) and aerosol components. The wavebands used in the retrieval are 440, 675, 870, 1020 nm. Using these data, PVSD and CRI sub-modal parameters of atmospheric aerosols are obtained using the modal decomposition method proposed by Zhang et al. (2017). Using the sub-modal characteristics data set thus obtained, an aerosol sub-modal model was established for China by Li et al. (2019), but the sub-modal aerosol components have not been given.

https://doi.org/10.5194/acp-2019-1062
Preprint. Discussion started: 22 January 2020

Atmospheric Chemistry and Physics Discussions

2.3 Meteorological data

Meteorological data provide important supplementary information for the analysis and interpretation of the SONET-retrieved aerosol information. Meteorological data were derived from hourly observations at surface meteorological stations provided by the China Meteorological Administration. To avoid observation uncertainties, only data from manned weather stations are used that are maintained regularly. The weather stations closest to the SONET site were selected, and the linear interpolation method is used to match the SONET observations (Table 1). Figure 2 shows the relative humidity (RH) statistics at 16 sites. The highest mean RH occurs at the Sanya site, and the lowest value at the Lhasa site. Generally, the mean RH is relatively low at stations at northern latitudes, and low RH also is often observed at high altitude. The standard deviations of wet (eg. Sanya, Haikou) and dry sites (eg. Lhasa, Kashgar) are smaller than at other sites. It is should be noted that retrieving aerosol components in the atmospheric column using the relative humidity only near the surface, in the absence of meteorological and aerosol profile observations, can introduce some uncertainty.

3. Methodology

We use a microphysical aerosol forward model including the Maxwell Garnett effective medium approximation (Schuster et al., 2005) module to calculate aerosol internal mixing characteristics, an aerosol hygroscopic growth module to solve the hygroscopicity of water-soluble components in a multicomponent liquid system, and an organic component dynamic constraint module in order to keep a reasonable ratio of organic matter. The aerosol microphysical properties calculated using the forward model are compared with those retrieved from the SONET observations (Zhang et al., 2017) to minimize the iterative kernel function.

3.1 The aerosol component classification

The aerosol component classification includes five principal species (black carbon (BC), organic matter (OM), inorganic salt (IS), aerosol water (AW), dust-like (DU) components). Three of these components are further sub-divided, i.e. organic matter is sub-divided into water-soluble (WSOM) and water-insoluble organic matter (WIOM), inorganic salt consists of ammonium nitrate (AN) in the fine mode and sodium chloride (SC) in the coarse mode, and aerosol water is the water content in the fine and in the coarse mode. Thus there are eight sub-components as illustrated in figure 3. All of these aerosol components constitute a relatively complete system comparable to those used in chemical transport models.

The aerosol components are identified following three steps. The first step is separation of the aerosol into fine and coarse mode. For fine mode, the water-insoluble and water-soluble components are identified using an empirical function (Zhang et al., 2018), and then the subcomponents are separated using their hygroscopic and optical absorption properties. For coarse mode, the refractive index of hydrate (AW_c and SC) is determined by hygroscopic growth, and then dust and hydrate in the

https://doi.org/10.5194/acp-2019-1062
Preprint. Discussion started: 22 January 2020

Atmospheric Chemistry and Physics Discussions

aerosol mixture are separated by the effective medium approximation. In these processes, the hygroscopic growth is determined by the parameter κ and effective densities of the aerosol subcomponents, and the aerosol mixture refractive index is calculated by that of the subcomponents and the mixing state. Key parameters of the forward model and references are listed in table 2. We notice that the effective densities for OC and DU reported from different studies cover a large range (Ganguly et al., 2009; McConnell et al., 2008; Wagner et al., 2012; Bond and Bergstrom, 2006) because they depend on the mixing ratios. We choose a widely cited study to obtain the effective density of aerosol components (Zhang et al., 1993).

3.2 Complex refractive index in a multicomponent liquid system

The multiple water-soluble aerosol components together with the aerosol water make up a liquid system, with increased complexity of the calculation of hygroscopic growth and complex refractive index. The κ-Köhler theory proposed by Petters and Kreidenweis (2007) can cope with the hygroscopicity of the multicomponent liquid system. In this theory, the water activity of aqueous atmospheric particulate matter can be represented by the functional form

$$\frac{1}{a_w} = 1 + \kappa \frac{V_s}{V_w} \tag{1}$$

where V_s is the volume of the dry particulate matter and V_w is the volume of the water. The activity of water in solution (a_w) can be replaced with RH, because it is close to the relative humidity (RH) due to lower curvature effect (Tang, 1996). The hygroscopicity parameter κ is defined through its effect on the water activity of the solution. In equation (1), the ratio of V_s to V_w can be further applied to the calculation of the volume fraction

$$y = \frac{V_s}{V_s + V_w} = \sum_i f_i = \frac{1 - a_w}{1 - (1 - \kappa)a_w} \tag{2}$$

where f_i is the volume fraction of the ith individual component

$$f_i = \frac{V_i}{V_s + V_w} \tag{3}$$

where V_i is the volume of the ith individual component.

In the multicomponent liquid system, the hygroscopicity parameter κ is given by the simple mixing rule

$$\kappa = \sum_i \varepsilon_i \kappa_i \tag{4}$$

where κ_i is the hygroscopic parameter of the ith individual component which can be computed by the hygroscopic growth factor, and ε_i is the dry component volume fraction defined as

https://doi.org/10.5194/acp-2019-1062
Preprint. Discussion started: 22 January 2020

Atmospheric Chemistry and Physics Discussions

$$\varepsilon_i = \frac{V_i}{V_s} \tag{5}$$

Using equation (2) for the relationship between the volume fraction and the hygroscopicity parameter, the complex refractive index of the multi-component aerosol system can be further derived from the Lorentz-Lorenz relation (Heller, 1965). Firstly, the molar refractivity (A_e) can be calculated from the refractive index and the volume fraction of the individual components

$$A_e = \sum_i f_i A_i \tag{6}$$

Where A_i is the molar refractivity of the ith individual component represented by

$$A_i = \frac{n_i^2 - 1}{n_i^2 + 2} \tag{7}$$

Then, the real and imaginary parts of the complex refractive index are obtained respectively by using the molar refractivity and the imaginary part of the complex refractive index of the ith individual component (k_i).

$$n_e = \sqrt{\frac{1 + 2A_e}{1 - A_e}} \tag{8}$$

$$k_e = \sum_i f_i k_i \tag{9}$$

Equations (8) and (9) apply to the estimation of the complex refractive index of a multi-component liquid system with hygroscopic growth.

3.3 Minimization procedure

In the particle, water-insoluble matter is regarded as inclusion and water-soluble matter as their environment. The Maxwell Garnett effective medium approximation (Schuster et al., 2005) is used to compute the effective permittivity of the particle in the fine or coarse mode,

$$\varepsilon_{eff}(\lambda) = \varepsilon_e + 3\varepsilon_e \left[\frac{\sum_j \frac{\varepsilon_j(\lambda) - \varepsilon_e(\lambda)}{\varepsilon_j(\lambda) + 2\varepsilon_e(\lambda)} f_j}{1 - \sum_j \frac{\varepsilon_j(\lambda) - \varepsilon_e(\lambda)}{\varepsilon_j(\lambda) + 2\varepsilon_e(\lambda)} f_j} \right] \tag{10}$$

Where, j is the number of water insoluble components and λ is the observed wavelength. $\varepsilon_j(\lambda)$ and $\varepsilon_e(\lambda)$ are the permittivities of the inclusion and its environment. Meanwhile, the complex refractive index (m=n-ki) in the fine or coarse mode can be

https://doi.org/10.5194/acp-2019-1062
Preprint. Discussion started: 22 January 2020

Atmospheric Chemistry and Physics Discussions

calculated from the permittivities.

$$m(\lambda) = \sqrt{\frac{|\varepsilon(\lambda)| + Re(\varepsilon(\lambda))}{2}} + i\sqrt{\frac{|\varepsilon(\lambda)| - Re(\varepsilon(\lambda))}{2}} \quad (11)$$

In order to minimize the residual at multiple wavelengths between the complex refractive index estimates from the forward model (m) and the retrievals (m_{rtrl}), the function of Chi-square (χ^2) as an iterative kernel function can be written as

$$\chi^2 = \sum_{\lambda} \frac{m_{rtrl}(\lambda) - m(\lambda)}{m_{rtrl}(\lambda)} \quad \lambda=440,\ 675,\ 870 \text{ and } 1020 \text{ nm} \quad (12)$$

For the minimum value of χ^2, the volume fraction of aerosol component can be obtained by solving the above equations (10-12). Then, its mass concentration in the atmospheric column is calculated using to the volume and effective density of the aerosol components.

3.4 Uncertainty analysis

In order to theoretically estimate the uncertainty of the inversion components, we choose three typical pollution cases in which the main pollutants are water soluble, biomass burning and dust aerosols, respectively, further referred to as WS, BB and DU pollution types. Each type is described by the different aerosol size distribution and refractive index parameters derived from Zhang et al. (2017). These parameters are listed in supplementary table S1. It should be noted that although the acronyms of the three pollution types are the same as the aerosol component names above, it does not mean that only a single aerosol component exists in this type.

Figure 4 shows the aerosol volume size distribution, complex refractive index and eight aerosol components in these types as benchmarks. For the size distribution, the highest volume concentrations occur in the fine mode of the WS and BB types, whereas for the DU type it is in the coarse mode. For the complex refractive index, significant absorption occurs in the fine mode of the BB type, while relatively low absorption occurs in the other models. In the WS type, the mass fraction of AW_f is close to 20% and for AN it is about 18%, significantly greater than for the other types. By comparison, the BC mass fraction in the BB type is close to 3%, and organic carbon is also high, with WSOM and WIOM mass fractions of 23% and 11%. In the DU type, the dust component is completely dominant, as expected, and the mass fractions of other components are less than 2%.

Three main sources of model input parameter uncertainties include the RH and the complex refractive index in the fine and coarse modes. The errors caused by the inversion algorithm of the modal refractive index were discussed in detail in Zhang et al. (2017) and are directly used here to estimate their effects on aerosol components. For RH, although WMO (2008) points out that its observation error is about 5%, here we introduce an even greater error (10%) to assess the uncertainty of estimated

https://doi.org/10.5194/acp-2019-1062
Preprint. Discussion started: 22 January 2020

Atmospheric Chemistry and Physics Discussions

aerosol components more rigorously. These typical uncertainties are listed in table S2. The total relative error (TRE), which is the propagated relative error calculated by the mean aerosol component error induced by the errors of sub-CRIs and RH in three pollution types, is used to assess the uncertainty of aerosol composition inversion. As shown in table 3, the TRE of BC is 32.21%, less than other components in the fine mode, and the largest source of TRE is the imaginary part of the complex refractive index (k_f), up to 18.57%. Compared with BC, the TRE of OM is larger (about 75%), primarily contributed by RH, followed by n_f. The uncertainty of the imaginary part impacts very little due to the low absorption of OM. Analogously, AN has low uncertainty caused by the imaginary part, but very high uncertainty caused by RH. Another component of IS is the SC which usually occurs in the coarse mode. The large TRE of SC is contributed by the real part of the complex refractive index in the coarse mode (n_c), up to 912.87%, leading to the largest TRE of IS. Affected by SC, the TRE of AW_c is also large due to n_c, but the TRE of AW_f is acceptable (50.05%). In the coarse mode, the TRE of DU is smallest in all of the aerosol components, only 15.79%, mainly caused by n_c. Overall, most of the uncertainties in the fine mode are from RH, and that in the coarse mode from the n_c. Fortunately, the RH observed by ground-based stations is accurate, with an error which is usually less than about 5% (WMO, 2008). The accuracy of the retrieved n_c needs to be improved in order to deal with the aerosol component inversion.

4. Results

4.1 Aerosol component retrievals

The averaged mass fractions of the aerosol components measured at 16 SONET sites are presented in Figure 5. Each subgraph is marked with the site name, location, and observation period. The pie charts show that the coarse mode mass fraction usually dominates (more than 50%) except for Guangzhou (44.4%), Haikou (44.6%) and Sanya (49.2%). The mass fraction of the dust component is significantly higher than that of others, with a fraction of more than 50% at the western (Lhasa, Zhangye, Kashgar, Minqin and Xi'an), Beijing and Songshan sites, which is different from surface observations of chemical components (Zhang et al., 2012; Liu et al., 2014). This is because the dust transport layer near 4 km (Proestakis et al., 2018) can be detected by remote sensing techniques which integrate over the whole atmospheric column, whereas surface observations are local point measurements. The lowest dust fractions are observed at southern sites, especially at the Guangzhou and Haikou sites, with a minimum of 20.1%. In contrast, the water content is dominant at southern sites in both the fine and coarse mode. The maximum water content (AW_f and AW_c) fraction occurs at the Haikou site (31.1%), and the minimum of 7.6% is observed at the Kashgar site. High AW_f occurs in the cities of east-central China due to the larger occurrence of inorganic salts with higher hygroscopicity in the fine mode at these sites, whereas the dominant AW_c in the western sites can be explained by the inorganic salt coating of larger particles in the dust source region (Rosenfeld et al., 2001). The inorganic salt fraction (AN and SC) gradually increases from north to south, which is consistent with the trend of the water content. The fraction of the AN sub-

https://doi.org/10.5194/acp-2019-1062
Preprint. Discussion started: 22 January 2020

component is less than 4% at Lhasa, Zhangye, Kashgar and Minqin, whereas it is more than 20% at Chengdu, Guangzhou, Haikou and Sanya. At the Zhoushan site also a high AN fraction is observed, up to 18.7%. For the SC component, the maximum values appear at both the Haikou (11.2%) and Kashgar (11.0%) sites. The high SC fraction in the southeast coastal sites is not difficult to understand, but the high SC fraction in Kashgar is because dust over the Taklimakan Desert had its paleo-marine source (Huang et al., 2010). The WIOM component fraction is high in the central sites but relatively low in the southern coastal and northwest sites. For the WSOM component, the low value appears only at northwest sites, with a minimum of 1.7% at Kashgar. In the atmospheric column, the mass fraction of the BC component averaged over 16 sites is only 0.61%, lower than from near-surface in situ observations (usually 1% ~ 5%), which implies that the BC fraction may be reduced by the suspended layer with other components such as dust aerosol. Nevertheless, the unusually higher mass fraction of BC in Shanghai could be due to observation uncertainty, also accompanied by the large error for aerosol component inversion. The mean error of the imaginary part of the complex refractive index at 675nm in Shanghai is up to 0.0123.

The closure of the complex refractive index between instantaneous optical-physical inversion and chemical estimation is examined by the data pair frequency. Figure 6 shows as an example the imaginary part of the fine mode (k_f); other parameters have similar features. The data pairs are concentrated around the 1:1 line, although the estimated values are on average 95.8% lower than the retrieved values, the mean bias is not large (-0.0032), whose absolute value is equal to the absolute error (AE = 0.0033). There are two reasons for this slight underestimation in chemical estimation. On one hand, the imaginary part of the refractive index of BC is significantly higher than for other components due to its strong absorption. Thus, the inversion of the BC concentration is very sensitive to the estimation of the refractive index. As shown in table 3, although the TRE of BC is the lowest, it also causes the largest k_f and $k_{f,440}$ errors. On the other hand, k_f is not only affected by BC in the inversion process, but also affected by organic components (WSOM & WIOM) with spectral absorption characteristics. Therefore, in most cases, k_f is underestimated in chemical estimation. Moreover, the mean relative error (RE) is 29.93%, and 61% of the data points is below the average relative error line. This indicates that most inversion results have good optical closure, and the aerosol components retrieved by the remote sensing method used in this study should be reasonable.

4.2 Seasonal variation

The seasonal variation of the aerosol component mass concentrations, averaged over 15 stations (except Lhasa due to lack of adequate seasonal data) and all available years, is shown as box-whisker plots in Figure 7. The top and bottom edges of each box represent the top and bottom quartiles (Q3 and Q1), and the corresponding whiskers are the outliers (Q3+1.5IQR and Q1-1.5IQR, IQR is interquartile range). The mean value is indicated by a plus sign (+), and the median value by a short line inside the box (–). Figure 7 shows that the DU component exhibits an obvious seasonality. The mass concentration of DU is very high in the spring and the mean value reaches up to 439.0 mg m^{-2} due to dust transport from northwest China. With the

https://doi.org/10.5194/acp-2019-1062
Preprint. Discussion started: 22 January 2020

weakening of dust transport and the increase of moisture, the DU fraction has a minimum in the summer, with a median value of 116.3 mg m^{-2}. However, the DU concentration near the dust source area is still relatively high in the summer, which results in a large difference between upper and lower quartiles. On the contrary, the AN mass concentration mean value peaks in the summer (68.3 mg m^{-2}), whereas a minimum occurs in the spring (47.9 mg m^{-2}). It is worth noting that although the mean value in the winter is not high (51.6 mg m^{-2}), the interval between the upper and lower quartiles of AN is the smallest in the winter. The minimum value of AN (22.7 mg m^{-2}) is higher than in other seasons (6.7 mg m^{-2} in spring, 7.6 mg m^{-2} in summer, and 10.4 mg m^{-2} in autumn). The seasonal variation of the water content is slightly different from that of inorganic salts. The low values of mean AW_f occur in the spring, while AW_c is significantly lower in the winter (22.6 mg m^{-2}) than in other seasons. The difference between the upper and lower quartile of AW_f in the summer is larger than in other seasons, indicating that the aerosol at some sites has a low hygroscopicity in the summer. OM mass concentration is slightly higher in the winter than that in other seasons probably due to the occurrence of haze pollution in the winter, with mean concentrations for WIOM and WSOM fractions of 29.3 and 35.5 mg m^{-2}, respectively. In the summer, the OM concentration is only about two thirds of that in the winter. The median value of the BC mass concentration is highest in the winter (3.1 mg m^{-2}) and second in autumn, which can be related to heating in northern China. Low concentrations of BC in the other two seasons are mainly due to the influence of frequent dust events in the autumn and high aerosol hygroscopic growth in the summer. Similar to AN, the SC concentration peaks in the summer and has a minimum in the winter, due to the influence of the Asian monsoon. The median values in these two seasons are respectively 33.4 and 20.9 mg m^{-2}.

4.3 Interannual variation

Figure 8 shows the interannual variations of the aerosol component mass concentrations in the atmospheric column from 2010-2016. The 16 SONET sites have been established in succession, so the number of available observations increased year by year with the longest time series from the Beijing site (see also Table 1). The annual mean mass concentration shown in Figure 8 is the average over all sites, i.e. the number of sites was not accounted for and, in particular in the earlier years (2010-2011), the annual mean may thus be representative for one (Beijing) or a few sites. Therefore, the annual means for each site available has been plotted as well. Figure 8 shows that the annual mean mass concentrations of most of the aerosol components in the fine mode increased in most of the first years and then decreased. Influenced by China's environmental control policies, the mean AN decreased significantly from 80.8 mg m^{-2} in 2011 to 54.0 mg m^{-2} in 2016, i.e. a reduction by 26.8 mg m^{-2}. The yearly mass concentrations of AN at most sites also follow a downward trend, and AN in the southeast coastal sites are significantly higher than that in the northwest sites. In contrast, the mean BC mass concentration shows a peak (4.3 mg m^{-2}) in 2011, drops in 2012 to the lowest value during the whole period (2.0 mg m^{-2}), then increases somewhat to a second peak (2.8 mg m^{-2}) in 2014. After a slight decrease in 2015, BC climbed to 2.6 mg m^{-2} again in 2016, the same as in 2010. In the southeast coastal

https://doi.org/10.5194/acp-2019-1062
Preprint. Discussion started: 22 January 2020

and northwest sites, BC concentration was relatively low. The two unusually high values at Nanjing in 2014 and Shanghai in 2016 may be due to observational errors. Similar to BC, AW_f also experienced a small fluctuation after a significant decline in 2012. The AW_f in aerosol measured in the south sites are higher than that in other sites. The fine mode WIOM and WSOM components show different behaviour. WIOM reached a peak in 2011 and 2013, with the peak value of 41.1mg m^{-2}, and then showed a significant decline after 2013. WSOM also had two peaks, with a peak concentration of 35.8 mg m^{-2} in 2013, which is 3 mg m^{-2} higher than the peak in 2011, and overall the concentrations increased. These results suggest that the policy of air pollution control in China is effective in controlling inorganic salts and WIOM aerosols, while WSOM still needs to be further controlled. The concentrations of the coarse mode aerosol components fluctuate somewhat during the observation period, with a slight peak in 2013. The concentration of each component in the coarse mode in the northwest sites is higher than that in other sites, which can be related to the high fraction of large particles. Due to the large influence of geographical factors on the coarse mode aerosol components, DU in 2010 (only Beijing site) was significantly larger than in other years. Since 2014, the mean DU mass concentration has increased. In the last two years, the AW_c shows an upward tendency, while the SC shows a downward tendency since 2013. Coarse mode aerosols usually derive from natural sources, and their variations can be associated with changes in meteorological conditions.

5. Conclusions and discussions

The accurate measurement of atmospheric aerosol components plays an important role in reducing the uncertainty of climate assessment. In the current study, we updated the refractive index calculation in a multi-component liquid system and improved a component inversion algorithm to retrieve atmospheric columnar aerosol components including black carbon (BC), organic matter (WSOM/WIOM), inorganic salt (AN & SC), dust-like (DU) and water content in the fine and coarse modes (AW_f & AW_c). This algorithm was applied to data from the SONET sun photometer network, and the regional distribution and interannual variation of atmospheric aerosol components in China were analyzed for the period from 2010 to 2016. The results show that the dust-like component is dominant in northern China, but the aerosol water content (AW_f & AW_c) is dominant in the southern coastal region. The inorganic salt (AN) in the fine mode has a significant seasonal variation, with a fraction of 19.2% in the summer which is significantly higher than that in other seasons. Meanwhile, the AN concentrations have significantly decreased from 2011 to 2016, which is inseparable from China's environmental control policies. However, the slight increase in WSOM and BC is still noteworthy.

As the aerosol concentrations in the atmospheric column obtained from the inversion of remote sensing data are different from those measured by in situ measurements near the surface, such as on-line aerosol mass spectrometers, the validation of the retrieval results is difficult. Proestakis et al. (2018) used Cloud-Aerosol Lidar with Orthogonal Polarization (CALIOP) data to analyze the distribution of mineral dust over China and the results show the higher concentration of the DU component in the

https://doi.org/10.5194/acp-2019-1062
Preprint. Discussion started: 22 January 2020

atmospheric column over northern China. Similarly, Huang et al. (2010) provided a basis for the high SC content at the Kashgar station due to the paleo-marine source. However, for the direct comparison of our retrievals with independent data, airborne measurements of the vertical distribution of atmospheric aerosol components are needed (Kahn et al., 2017). In future research, we will design a verification experiment to comprehensively evaluate the results from our inversion method.

This method can be used not only for ground-based sun-sky photometer measurements, but also for other remote sensing instruments (e.g. lidar), and even for satellite remote sensing in the future. Meanwhile, as long as measurements of multi-wavelength extinction coefficients and aerosol particle size distributions are available, the inversion of atmospheric particulate matter composition can also be performed using comprehensive observations with multiple instruments near the surface. Therefore, this method can be widely used in low-cost and wide-area measurements in the future, providing a possibility for obtaining the global distribution of aerosol composition.

Data availability. The aerosol component data used in this study can be requested from the corresponding author (lizq@radi.ac.cn).

Author contributions. ZL conceived and designed the study. YC collected and processed the meteorological data. KL and YX collected the remote sensing data. CZ collected the DEM data and draw the map. YZ improved the aerosol component method and performed the inversions. YZ analyzed the spatiotemporal trends of aerosol component concentrations. YZ and GL prepared the paper with contributions from all coauthors.

Acknowledgments. This work was supported by the National Key R&D Program of China (grant 2016YFE0201400) and the National Natural Science Fund of China (41601386).

References

Arola, A., Schuster, G., Myhre, G., Kazadzis, S., Dey, S., and Tripathi, S. N.: Inferring absorbing organic carbon content from AERONET data, Atmospheric chemistry and physics, 11(1), 215– 225, 2011.

Bond, T. and Bergstrom, R.: Light absorption by carbonaceous particles: an investigative review, Aerosol Science and Technology, 40, 27–67, 2006.

Boucher, O., Randall, D., Artaxo, P., Bretherton, C., Feingold, G., Forster, P., Kerminen, V.-M., Kondo, Y., Liao, H., Lohmann, U., Rasch, P., Satheesh, S.K., Sherwood, S., Stevens, B. and Zhang, X.Y.: Clouds and Aerosols. In: Climate Change 2013: The Physical Science Basis. Contribution of Working Group I to the Fifth Assessment Report of the Intergovernmental Panel on Climate Change [Stocker, T.F., D. Qin, G.-K. Plattner, M. Tignor, S.K. Allen, J. Boschung, A. Nauels, Y. Xia, V. Bex and P.M. Midgley (eds.)]. Cambridge University Press, Cambridge, United Kingdom and New York, NY, USA, 2013.

Chen, Y. and Bond, T. C.: Light absorption by organic carbon from wood combustion, Atmos. Chem. Phys., 10, 1773–1787, doi:10.5194/acp-10-1773-2010, 2010.

https://doi.org/10.5194/acp-2019-1062
Preprint. Discussion started: 22 January 2020

Choi, Y. and Ghim, Y. S.: Estimation of columnar concentrations of absorbing and scattering fine mode aerosol components using AERONET data, Journal of Geophysical Research Atmospheres, 121, 13628-13640, 2016.

Dubovik, O., Smirnov, A., Holben, B.N., King, M.D., Kaufman, Y.J., Eck, T.F., Slutsker, I.: Accuracy assessments of aerosol optical properties retrieved from aerosol robotic network (AERONET) Sun and sky radiance measurements. J. Geophys. Res. Atmos. 105, 9791-9806, 2000.

Ganguly, D., Ginoux, P., Ramaswamy, V., Dubovik, O., Welton, J., Reid, E. A. and Holben, B. N.: Inferring the composition and concentration of aerosols by combining AERONET and MPLNET data: Comparison with other measurements and utilization to evaluate GCM output, J Geophys Res-Atmos, 114(D16), 2009.

Heller, W., Remarks on refractive index mixture rules, The Journal of Physical Chemistry, 69(4), 1123-1129, 1965.

Huang, K., Zhuang, G., Li, J., Wang, Q., Sun, Y., Lin, Y and Fu, J. S.: Mixing of Asian dust with pollution aerosol and the transformation of aerosol components during the dust storm over China in spring 2007, J. Geophys. Res., 115, D00K13, doi:10.1029/2009JD013145, 2010.

Kahn, R.A., Berkoff, T.A., Brock, C., Chen, G., Ferrare, R.A., Ghan, S., Hansico, T.F., Hegg, D.A., Vanderlei Martins, J., McNaughton, C.S., Murphy, D.M., Ogren, J.A., Penner, J.E., Pilewskie, P., Seinfeld, J.H., and Worsnop, D.R.: SAM-CAAM: A Concept for Acquiring Systematic Aircraft Measurements to Characterize Aerosol Air Masse," Bull. Amer. Meteor. Soc., 98, 2215–2228) doi:10.1175/BAMS-D-16-0003.2, 2017.

Kreidenwies S. M., Petters, M. D. and DeMott, P.: Single-parameter estimates of aerosol water content, Environ. Res. Lett., 3, 035002, 1-7, 2008.

Koven, C. and Fung, I.: Inferring dust composition from wavelength-dependent absorption in Aerosol Robotic Network AERONET data, J. Geophys. Res., 111, D14205, doi:10.1029/2005JD006678, 2006.

Lesins, G., Chylek, P., and Lohmann, U.: A study of internal and external mixing scenarios and its effect on aerosol optical properties and direct radiative forcing, J Geophys Res-Atmos, 107(D10), 2002.

Li, L., Dubovik, O., Derimian, Y., Schuster, G. L., Lapyonok, T., Litvinov, P., Ducos, F., Fuertes, D., Chen, C., Li, Z., Lopatin, A., Torres, B. and Che, H.: Retrieval of aerosol components directly from satellite and ground-based measurements, Atmos. Chem. Phys., 19, 13409–13443, 2019.

Li, Z., Zhang, Y., Xu, H., Li, K., Dubovik, O., and Goloub, P.: The fundamental aerosol models over China region: A cluster analysis of the ground-based remote sensing measurements of total columnar atmosphere. Geophysical Research Letters, 46. https://doi.org/10.1029/2019GL082056, 2019.

Li, Z. Q., Xu, H., Li, K. T., Li, D. H., Xie, Y. S., Li, L., et al.: Comprehensive study of optical, physical, chemical, and radiative properties of total columnar atmospheric aerosols over China: An overview of Sun–Sky Radiometer Observation Network (SONET) measurements. Bulletin of the American Meteorological Society, 99(4), 739–755, 2018.

Li, Z., Gu, X., Wang, L., Li, D., Xie, Y., Li, K., Dubovik, O., Schuster, G., Goloub, P., Zhang, Y., Li, L., Ma, Y., and Xu, H.: Aerosol physical and chemical properties retrieved from ground-based remote sensing measurements during heavy haze days in Beijing winter, Atmospheric Chemistry and Physics, 13, 10171-10183, 2013.

Liu, Q., Liu, Y., Yin, J., Zhang, M. and Zhang, T.: Chemical characteristics and source apportionment of PM_{10} during Asian dust storm and non-dust storm days in Beijing, Atmospheric Environment, 91, 85-94, 2014.

McConnell, C. L., Highwood, E. J., Coe, H., Formenti, P., Anderson, B., Osborne, S., Nava, S., Desboeufs, K., Chen, G. and Harrison, M. A. J.: Seasonal variations of the physical and optical characteristics of Saharan dust: Results from the Dust Outflow and Deposition to the Ocean (DODO) experiment, J Geophys Res-Atmos, 113, D14S05, doi:10.1029/2007JD009606, 2008.

https://doi.org/10.5194/acp-2019-1062
Preprint. Discussion started: 22 January 2020

Petters M. D. and Kreidenweis S. M.: A single parameter representation of hygroscopic growth and cloud condensation nucleus activity, Atmospheric Chemistry and Physics, 7, 1961–1971, 2007.

Proestakis, E., Amiridis, V., Marinou, E., Georgoulias, A. K., Solomons, S., Kazadzis, S., Chimot, J., Che, H., Alexandri, G., Binietoglou, I., Daskalopoulou, V., Kourtidis, K. A., de Leeuw, G. and van der, A R. J.: Nine-year spatial and temporal evolution of desert dust aerosols over South and East Asia as revealed by CALIOP, Atmos. Chem. Phys., 18, 1337¨C1362, 2018.

Rosenfeld, D., Rudich, Y. and Lahav, R.: Desert dust suppressing precipitation: a possible desertification feedback loop, Proceedings of the National Academy of Sciences of the United States of America, 98(11), 5975-5980, 2001.

Satheesh, S. K. and Krishna, M. K.: Radiative effects of natural aerosols: A review, Atmospheric Environment, 39(11), 2089-2110, 2005.

Satheesh, S. K. and Srinivasan, J.: Enhanced aerosol loading over Arabian Sea during the pre-monsoon season: Natural or anthropogenic. Geophysical Research Letters, 29(18), 211-214, 2002a.

Satheesh, S. K., Ramanathan, V., Holben, B. N., Moorthy, K. K., Loeb, N. G., Maring, H., Prospero, J. M., and Savoie, D.: Chemical, microphysical, and radiative effects of Indian Ocean aerosols, Journal of Geophysical Research, 107(D23), 4725, 2002b.

Satheesh, S. K., Ramanathan, V., Li-Jones, X., Lobert, J. M., Podgorny, I. A., Prospero, J. M., Holben, B. N., and Loeb, N. G.: A model for the natural and anthropogenic aerosols over the tropical Indian Ocean derived from Indian Ocean Experiment data, Journal of Geophysical Research, 104(D22), 27421-27440, 1999.

Schuster, G. L., Dubovik, O., and Arola, A.: Remote sensing of soot carbon – Part 1: Distinguishing different absorbing aerosol species, Atmospheric chemistry and physics, 16, 1565-1585, 2016.

Schuster, G. L., Lin, B., and Dubovik, O.: Remote sensing of aerosol water uptake, Geophysical Research Letters, 36, L03814, doi:10.1029/2008GL036576, 2009.

Schuster, G. L., Dubovik, O., Holben, B. N., and Clothiaux, E. E.: Inferring black carbon content and specific absorption from Aerosol Robotic Network (AERONET) aerosol retrievals, Journal of Geophysical Research, 110, D10S17, doi:10.1029/2004JD004548, 2005.

Sun, H., Biedermann, L., and Bond, T.: Color of brown carbon: a model for ultraviolet 20 and visible light absorption by organic carbon aerosol, Geophys. Res. Lett., 34, L17813, doi:10.1029/2007GL029797, 2007.

Tang, I. N.: Chemical and size effects of hygroscopic aerosol on light scattering coefficients, Journal of Geophysical Research, 101(D14), 19245-19250, 1996.

Toon, O. B. and Pollack, J. B.: The optical constants of several atmospheric aerosol species: Ammonium sulfate, aluminum oxide, and sodium chloride, Journal of Geophysical Research, 81(33), 5733-5748, 1976.

van Beelen, A. J., Roelofs, G. J. H., Hasekamp, O. P., Henzing, J. S., and Rockmann, T.: Estimation of aerosol water and chemical composition from AERONET Sun-sky radiometer measurements at Cabauw, the Netherlands, Atmos. Chem. Phys., 14(12), 5969–5987, doi:10.5194/acp-14-5969-2014, 2014.

Wagner, R., Ajtai, T., Kandler, K., Lieke, K., Linke, C., Müller, T., Schnaiter, M., and Vragel, M.: Complex refractive indices of Saharan dust samples at visible and near UV wavelengths: a laboratory study, Atmospheric Chemistry Physics, 12, 2491–2512, 2012.

Wang, L., Li, Z. Q., Tian, Q. J., Ma, Y., Zhang, F. X., Zhang, Y., Li, D. H., Li, K. T., and Li, L.: Estimate of aerosol absorbing components of black carbon, brown carbon, and dust from ground-based remote sensing data of sun-sky radiometers, Journal of Geophysical Research, 118, 6534-6543, 2013.

https://doi.org/10.5194/acp-2019-1062
Preprint. Discussion started: 22 January 2020

WMO, 2008. Guide to Meteorological Instruments and Methods of Observation, seventh ed. (WMO No.8).

Xie, Y., Li, Z., Zhang, Y.X., Zhang, Y., Li, D. H., Li, K. T. Xu, H., Zhang, Y., Wang, Y. Q., Chen, X. F., Schauer, J. J., Bergin, M.: Estimation of atmospheric aerosol composition from ground-based remote sensing measurements of Sun-sky radiometer, Journal of Geophysical Research Atmospheres, doi: 10.1002/2016JD025839, 2017.

435 Zhang, X.Q., Mcmurry, P.H., Hering, S.V., Casuccio, G.S.: Mixing characteristics and water content of submicron aerosols measured in Los Angeles and at the Grand Canyon. Atmos. Environ. 27A (10), 1593–1607, 1993.

Zhang, X. Y., Wang, Y. Q., Niu, T., Zhang, X. C., Gong, S. L., Zhang, Y. M. and Sun, J. Y.: Atmospheric aerosol compositions in China: spatial/temporal variability, chemical signature, regional haze distribution and comparisons with global aerosols, Atmos. Chem. Phys., 12, 779–799, 2012.

440 Zhang, Y., Li, Z., Zhang, Y. H., Li, D., Qie, L., Che, H., and Xu, H.: Estimation of aerosol complex refractive indices for both fine and coarse modes simultaneously based on AERONET remote sensing products, Atmospheric Measurement Techniques, 10, 3203-3213, 2017.

Zhang, Y., Li, Z., Sun, Y., Lv, Y., Xie, Y.: Estimation of atmospheric columnar organic matter (OM) mass concentration from remote sensing measurements of aerosol spectral refractive indices, Atmospheric Environment, 179, 107-117, 2018.

445

https://doi.org/10.5194/acp-2019-1062
Preprint. Discussion started: 22 January 2020

Atmospheric Chemistry and Physics Discussions

Table 1. Observation period and geographic feature of 16 long-term sites of SONET network.

SONET Site						Meteorological Station					
Name	**Abbr**	**Lon (°)**	**Lat (°)**	**Alt (m)**	**Obs Period**	**No**	**Lon (°)**	**Lat (°)**	**Alt (m)**	**Geo feature**	**Geo region**
Lhasa	LS	91.2	29.6	3678	2016.03-2016.05	55591	91.1	29.7	3649	Plateau	Qinghai-Tibetan
Kashi	KS	75.9	39.5	1320	2013.09-2016.11	51709	76.0	39.5	1289	Desert	Northwest
Zhangye	ZY	100.3	38.8	1364	2012.08-2016.10	52652	100.4	38.9	1483	Gobi & desert	
Minqin	MQ	103.0	38.6	1589	2012.02-2016.10	52681	103.1	38.6	1368	Desert & hill	
Xi'an	XA	108.9	34.2	389	2012.05-2016.11	57039	108.9	34.2	433	Half mountain, half plain	
Beijing	BJ	116.3	40.0	59	2009.12-2016.11	54399	116.3	40.0	46	Hill (megacity)	Northern
Harbin	HrB	126.6	45.7	223	2013.12-2016.11	50953	126.8	45.8	118	Plain	
Songshan	SS	113.1	34.5	475	2013.12-2016.11	57084	113.1	34.5	1178	Mountain & hill	
Nanjing	NJ	119.0	32.1	52	2013.01-2016.07	58238	118.8	32.0	35	Plain & hill	Southern
Shanghai	SH	121.5	31.3	84	2013.03-2016.04	58362	121.5	31.4	6	Alluvial plain (megacity)	
Hefei	HF	117.2	31.9	36	2013.11-2016.11	58321	117.2	31.9	27	Hill	
Zhoushan	ZS	122.1	29.9	29	2012.02-2016.11	58477	122.1	30.0	36	Islands	
Chengdu	CD	104.0	30.6	510	2013.06-2016.07	56276	103.8	30.4	461	Basin	
Guangzhou	GZ	113.4	23.1	28	2011.10-2016.11	59287	113.3	23.2	41	Mountain, hill & plain (megacity)	
Haikou	HK	110.3	20.0	22	2014.03-2016.03	59758	110.3	20.0	64	Island	
Sanya	SY	109.4	18.3	29	2014.09-2016.11	59948	109.5	18.2	419	Island	

https://doi.org/10.5194/acp-2019-1062
Preprint. Discussion started: 22 January 2020

Atmospheric Chemistry and Physics Discussions

Table 2. Growth factor derived hygroscopic parameter (κ), complex refractive indexes ($m = n - ik$) for four wavelengths and effective density (ρ) of model components. Real and imaginary parts at four standard AERONET aerosol product wavelengths (440, 675, 870 and 1020 nm) are considered.

Component		Growth factor derived κ	Real Part				Imaginary Part		ρ (g cm^{-3})
			n_{440}	n_{675}	n_{870}	n_{1020}	k_{440}	$k_{675\sim1020}$	
OM	WIOM	0.000	1.530[c]	1.530	1.530	1.530	0.035[d]	0.001	1.547[i]
	WSOM	0.000[a]	1.530[c]	1.530	1.530	1.530	0.006[d]	0.000	
AN		0.547[b]	1.559[e]	1.553	1.550	1.548	0.000[e]	0.000	1.760[i]
BC		0.000	1.950[f]	1.950	1.950	1.950	0.790[f]	0.790	1.800[i]
AW		0.000	1.337[e]	1.332	1.330	1.328	0.000[g]	0.000	1.000[i]
DU		0.000	1.534[g]	1.534	1.534	1.534	0.002[h]	0.001	2.650[i]
SC		1.120[a]	1.562[h]	1.541	1.534	1.530	0.000[i]	0.000	2.165[i]

[a] Petters and Kreidenweis, 2007; [b] Kreidenweis et al., 2008; [c] Sun et al., 2007; [d] Chen and Bond, 2010; [e] Schuster et al., 2005; [f] Bond and Bergstrom, 2006; [g] Koven and Fung, 2006; [h] Toon et al., 1976; [i] Zhang et al., 1993.

https://doi.org/10.5194/acp-2019-1062
Preprint. Discussion started: 22 January 2020

Atmospheric Chemistry and Physics Discussions

Table 3. Estimated total relative errors (TRE) of aerosol component mass fractions in the three typical aerosol models.

Aerosol components		RH	Fine mode			Coarse mode			TRE*	
			n_f	$k_{f,440}$	k_f	n_c	$k_{c,440}$	k_c		
BC		5.74%	0.59%	25.68%	18.57%	0.00%	0.00%	0.00%	32.21%	
OM	WIOM	75.82%	4.55%	5.28%	1.08%	0.00%	0.00%	0.00%	76.15%	74.73%
	WSOM	51.60%	51.92%	3.44%	2.11%	0.00%	0.00%	0.00%	73.31%	
IS	AN	207.00%	60.86%	7.07%	6.04%	0.00%	0.00%	0.00%	215.96%	564.42%
	SC	25.71%	0.00%	0.00%	0.00%	912.51%	2.16%	1.23%	912.87%	
AW	AW_f	49.77%	3.80%	3.71%	0.00%	0.00%	0.00%	0.00%	50.05%	481.32%
	AW_c	8.95%	0.00%	0.00%	0.00%	912.55%	2.10%	1.17%	912.60%	
DU		0.34%	0.00%	0.00%	0.00%	15.78%	0.04%	0.02%	15.79%	

*TRE $= \sqrt{\sum_1^7 \bar{x}_i^2}$, where $\bar{x}$ represents the mean error of aerosol components from three aerosol types. The RH is given input error of ±10% and the inversion errors of sub-CRIs is from Table 2 in Zhang et al., 2017.

460

https://doi.org/10.5194/acp-2019-1062
Preprint. Discussion started: 22 January 2020

Atmospheric Chemistry and Physics Discussions

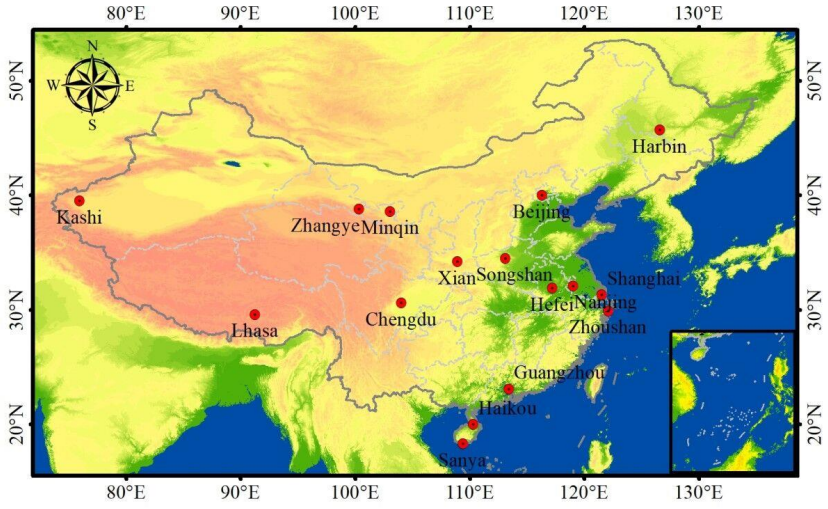

Figure 1. Locations of the 16 Sun-sky radiometer observation network (SONET) site project on the elevation map of China.

https://doi.org/10.5194/acp-2019-1062
Preprint. Discussion started: 22 January 2020

Atmospheric Chemistry and Physics Discussions

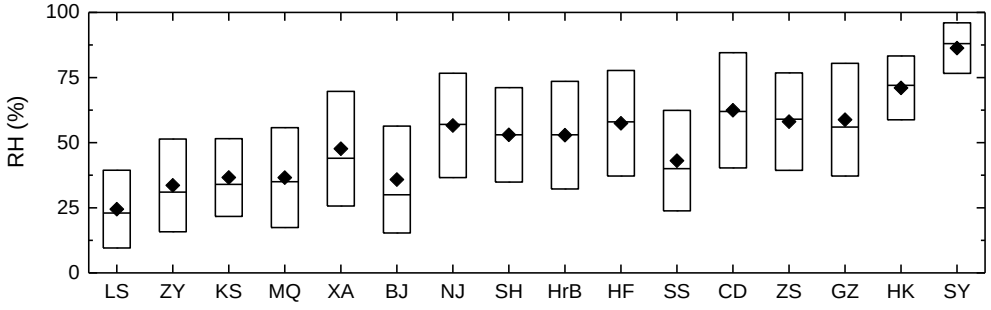

Figure 2. Box-whisker plot of relative humidity near SONET sites. The box shows the standard deviation; the middle line and point in the box present the median and mean values, respectively.

https://doi.org/10.5194/acp-2019-1062
Preprint. Discussion started: 22 January 2020

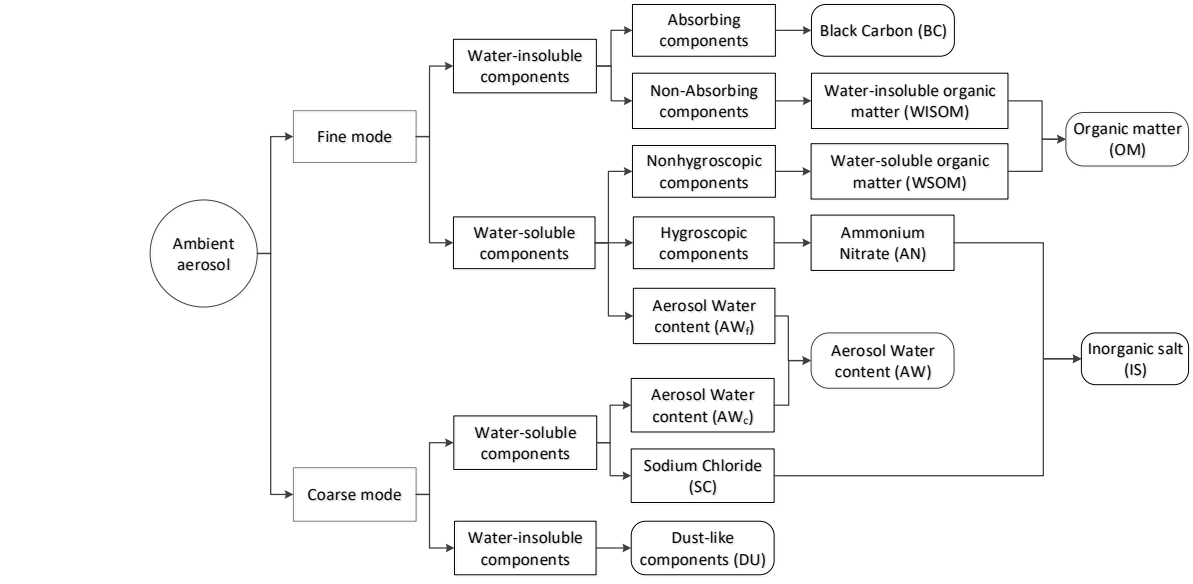

Figure 3. Flowchart of the aerosol component classification inversion algorithm.

475

https://doi.org/10.5194/acp-2019-1062
Preprint. Discussion started: 22 January 2020

Atmospheric Chemistry and Physics Discussions

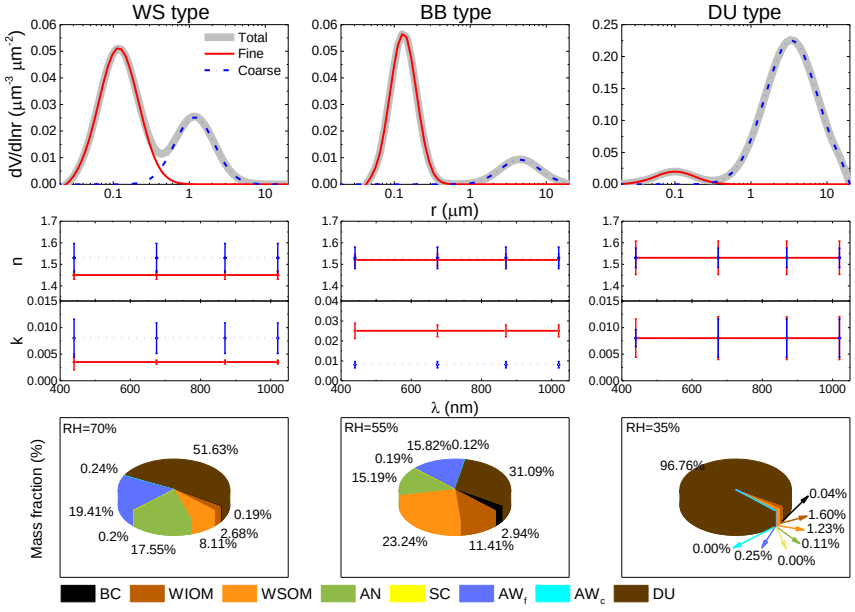

Figure 4. The fine and coarse-mode volume size distribution, complex refractive index and aerosol components of three typical aerosol models (WS: water soluble, BB: biomass burning, DU: dust).

480

https://doi.org/10.5194/acp-2019-1062
Preprint. Discussion started: 22 January 2020

Atmospheric Chemistry and Physics Discussions

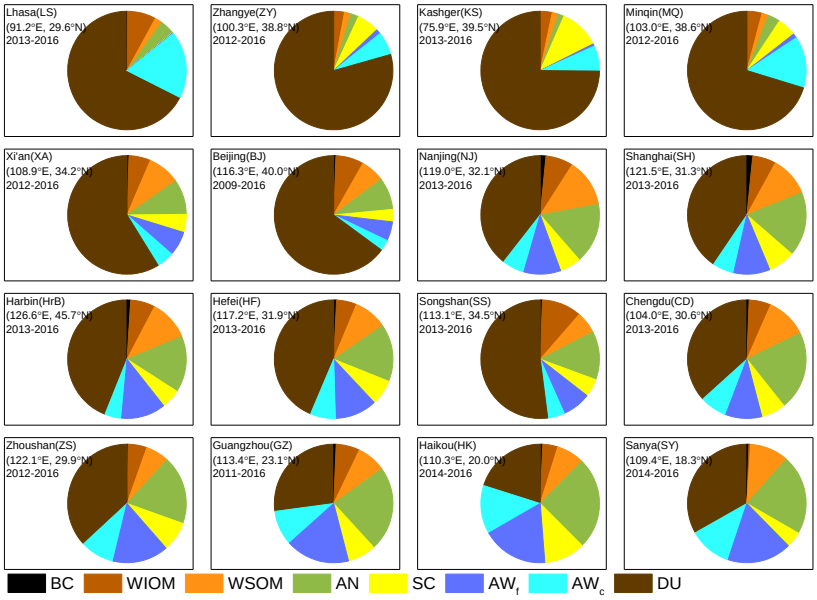

Figure 5. The averaged mass fraction of aerosol components at SONET sites. The site name, location, and observation period are marked in each subgraph.

https://doi.org/10.5194/acp-2019-1062
Preprint. Discussion started: 22 January 2020

Atmospheric Chemistry and Physics Discussions

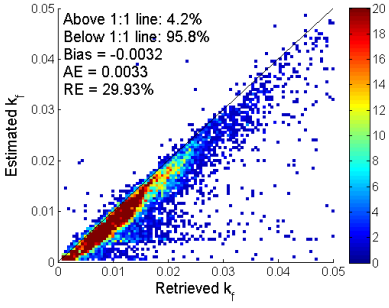

490 **Figure 6**. Data pair frequency of instantaneous imaginary part of the complex refractive index at 675 nm (k_f) which are sorted according to ordered pairs (Retrieved k_f, Estimated k_f) in 0.0005 intervals. "Retrieved k_f" represents k_f from the optical-physical retrievals, and "Estimated k_f" is estimated by retrieved chemical components. The color represents the number of cases (color bar), and the solid black line shows the 1:1 line.

495

https://doi.org/10.5194/acp-2019-1062
Preprint. Discussion started: 22 January 2020

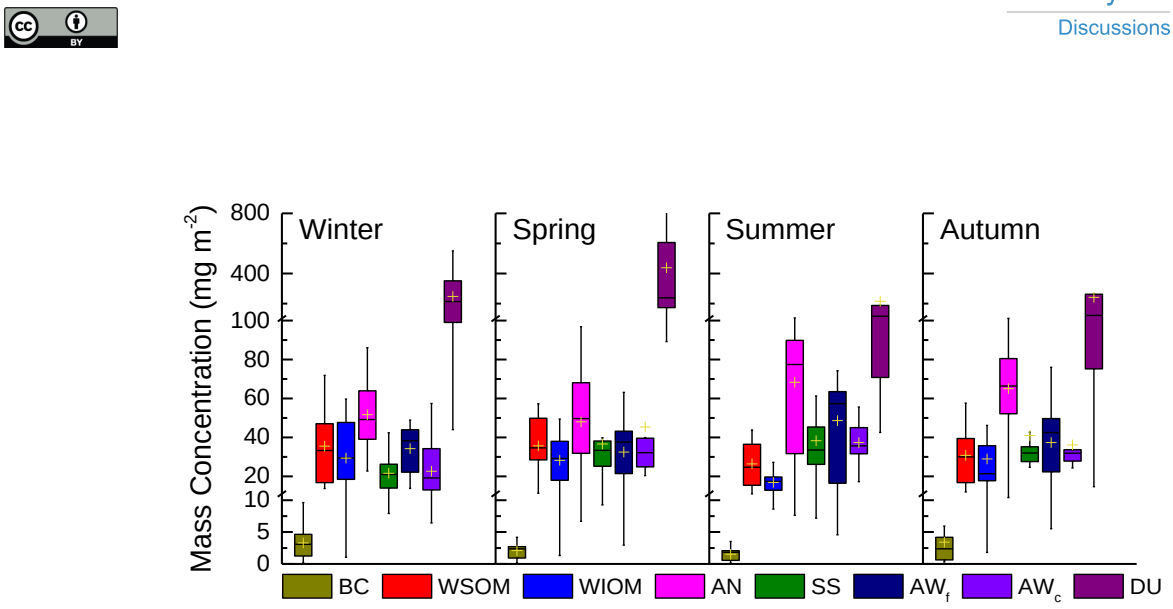

Figure 7. The mass concentrations of aerosol components in four seasons (winter, spring, summer and autumn). For the box-whisker plot, the mean value is indicated by a plus sign (+), and the median value by a short line inside the box (–). The top and bottom edges of box represent the top and bottom quartiles (Q3 and Q1), and the corresponding whiskers are the outliers (Q3+1.5IQR and Q1-1.5IQR, IQR is interquartile range).

https://doi.org/10.5194/acp-2019-1062
Preprint. Discussion started: 22 January 2020

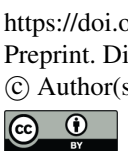

Atmospheric Chemistry and Physics Discussions

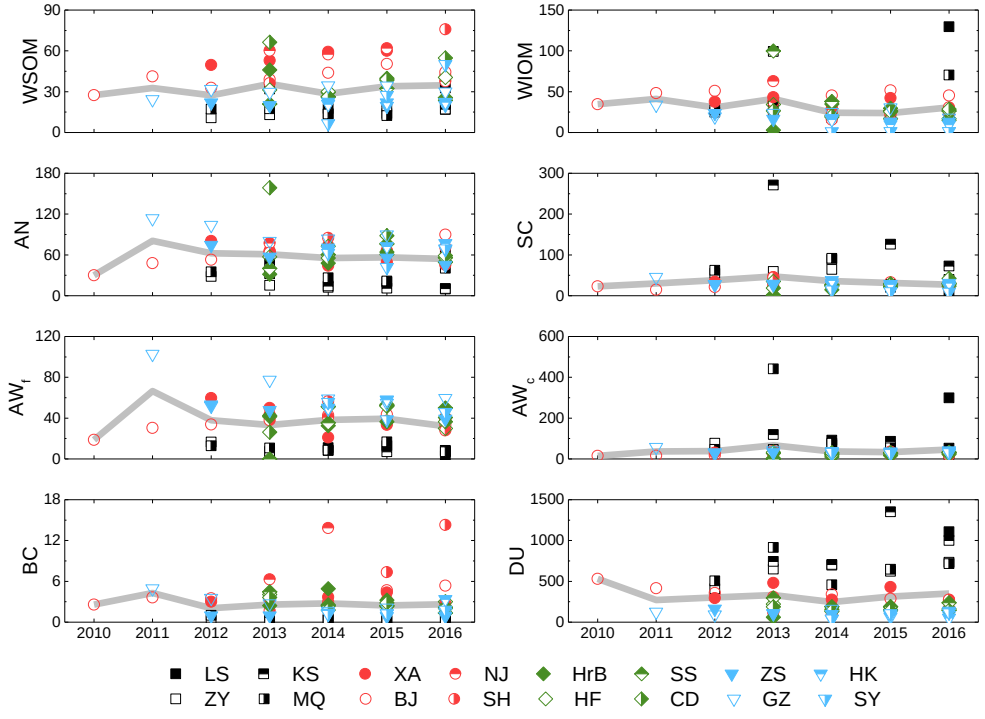

505

Figure 8. The interannual variations of mean aerosol component mass concentrations in atmospheric column with SONET sites from 2010-2016. The gray line represents the mean mass concentration of aerosol components averaged by the 16 sites; the points in subgraph show the yearly value at each site.

510